Proceedings of the ASME 2016 International Design Engineering Technical Conferences & Computers and Information in Engineering Conference
IDETC/CIE 2016
August 21-24, 2016, Charlotte, North Carolina

DETC2016-60261

AN ORIGAMI-INSPIRED, SMA ACTUATED LIFTING STRUCTURE

[†]Leo J. Wood leo.w@tamu.edu
[‡]Jaime Rendon jaime.rendon@tamu.edu
[†]Richard J. Malak rmalak@tamu.edu
[‡]Darren Hartl darren.hartl@tamu.edu

Design Systems Laboratory
[†]Department of Mechanical Engineering [‡]Department of Aerospace Engineering
Texas A&M University
College Station, Texas, 77843

ABSTRACT

Origami engineering is the study of the construction principles found in the art of origami and application of those principles to various engineering applications. Although origami engineering researchers have addressed the tasks of lifting a load and supporting a static load, to our knowledge no one has demonstrated a system combining these two important capabilities. In this paper, we describe an origami-inspired actuator that can fold flat, lift a load, and then support that load structurally with no electrical or mechanical input. The design is based on a bistable origami pattern similar to the classical origami waterbomb base, and is actuated by shape memory alloy (SMA) wires in torsion. We detail a framework for the generalized structure and actuation method of SMA wires as well as the construction and testing of a proof-of-concept lifter. This proof of concept structure, weighing 22 grams, is able to lift a 50g load in 8 seconds using a 2.5 Volt input, and statically support 200g even after the cessation of voltage input. We conduct a preliminary analysis into the parameters of the structure that most affect its lifting capabilities.

1 INTRODUCTION

Origami, the ancient art of paper folding, is in its purest form the practice of using a single sheet of paper to create intricate and varied structures, models, and works of art. This practice has captured the interest of engineering practitioners due to its impressive design potential; origami offers novel ways for structures to assemble and collapse, and has been shown to be a powerful tool for improving closely-packed or deployable devices like solar panels and airbags [1, 2] or laying the foundations for new deployable, stiff structures [3]. When one considers the possibility of origami designs and structures that can actuate and fold themselves, the applications and areas in which origami engineering can be used extend even farther; designing shape-changing wheels [4], creating robots that can be folded from flat, printed sheets [5], or even “sheets” of material that can fold and unfold themselves into a variety of designs [6]. The latter three examples all use Shape Memory Alloys (SMAs) to perform this self-folding; active materials like SMAs are frequently used to accomplish self-folding, as they provide a high energy density in a compact, geometrically simple form [7].

The use of origami in design brings elements of light weight, low profile, and reconfigurable construction—qualities that can be desirable for a lifting mechanism or actuator in many situations where space and weight are at a premium. In the past, origami-inspired lifting mechanisms have been considered, the most notable being that of a pneumatic pleated tube [8]. These designs, however, operate more as foldable hydraulic pistons than as self-folding origami designs. Furthermore, they cannot support a static load using their fold structure alone, requiring input pressure to operate. Origami-inspired designs that can support a static load have been investigated [9, 10], but these are static designs that cannot themselves perform useful work in lifting a mass. Essentially, in terms of using self-folding to perform useful work as an actuator, few designs exist, and no designs have solved the problem of performing useful work while still being able to freely support load using their structure alone.

This paper outlines a novel design for an origami-inspired lifting mechanism intended to fill the gap in origami engineering between lifting actuation and static support. By adapting the bistable nature of the waterbomb origami base into

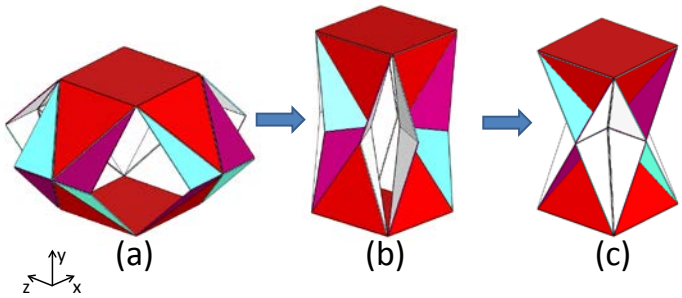

Figure 1. DEPICTION OF LIFTING STRUCTURE IN (a) FULLY OPEN, (b) LOCKED, AND (c) COMPRESSED STATES. COLORED PANELS ARE RIGID, WHILE WHITE UNDERSIDE IS A FOLDABLE SUBSTRATE

a structure of rigid panels and flexible folds with embedded active materials to provide lifting force, we produce a structure that can both lift a load in one configuration and statically support a load with no power input in another configuration. We present a generalized design for this structure, a modeling approach and analysis of important parameters in the structures design, and finally testing of an open-loop controlled physical prototype that was constructed and operated.

2 DESIGN OVERVIEW

Figure 1 is an illustration of the proposed origami-inspired lifter in its (a) fully open, (b) locked, and (c) compressed states. It consists of four identical and vertically symmetric sides possessing a specific fold pattern, attached to two identical square bases to form a shape similar to a prism. The underlying construction of the structure is that of a flexible, paper-like substrate to provide the folds and rigid panels attached on top of the substrate for reinforcement. The art of origami requires that a design be fully developable, i.e. capable of unfolding to a single sheet; the assembled structure, although capable of folding flat in the open state, is not developable, thus it is merely origami *inspired*.

To provide lifting torque, SMA wires are embedded into the structure along the *X* and *Z* direction base folds connecting the sides to the polygon bases. The wires are operated in torsion by pre-straining them opposite the desired rotational direction so that, upon phase transformation, they apply a torque in the direction required to lift the structure (Figure 3). SMA wire is commercially available and simple to operate in torsion, and it integrates well into origami folds as a low-profile means to produce lifting torque without bulky mechanisms that would be needed to employ the wires in a tensile mode, as is commonly done. By providing electrical current to induce joule heating in the wire, the SMA produces a torque that can be tied to a variety of control systems.

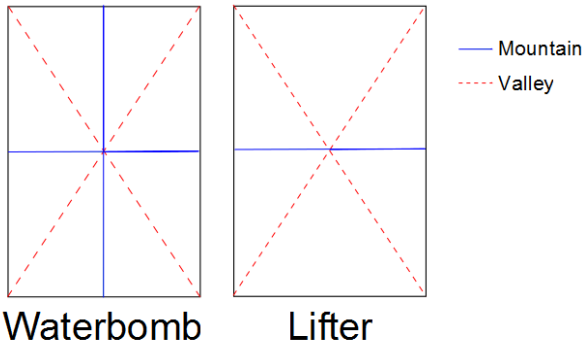

Figure 2. COMPARISON OF FOLD PATTERNS BETWEEN SINGLE LATERAL SIDE OF CURRENT DESIGN AND CONVENTIONAL WATERBOMB BASE

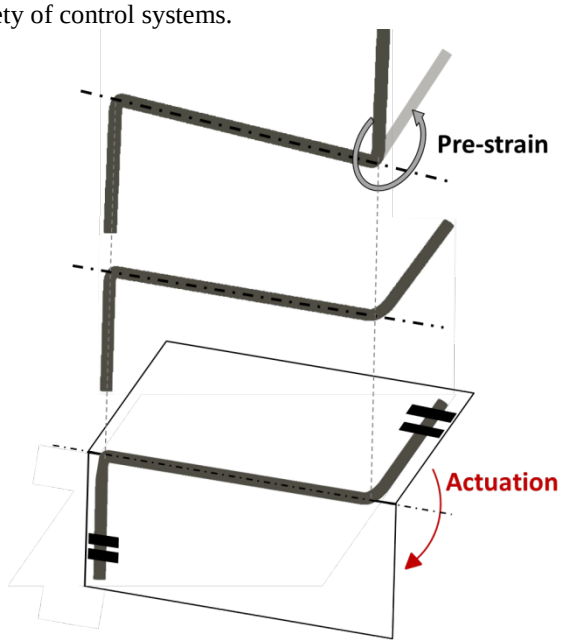

Figure 3. PRESTRAIN AND EMBEDDING OF SMA WIRE INTO EXAMPLE FOLD. HASH MARKS INDICATE ATTACHMENT POINTS

3 STRUCTURE AND GEOMETRY

The fold pattern for each lateral side is detailed in Figure 2. Similar designs with this fold pattern have been explored before [11], including an experiment using the fold pattern to create an articulating platform [12], but none have exploited the relation this fold pattern shares with a classic origami base, the waterbomb, and its resulting bistable nature. This pattern has two stable states (Figure 4)—open, and locked. When in the

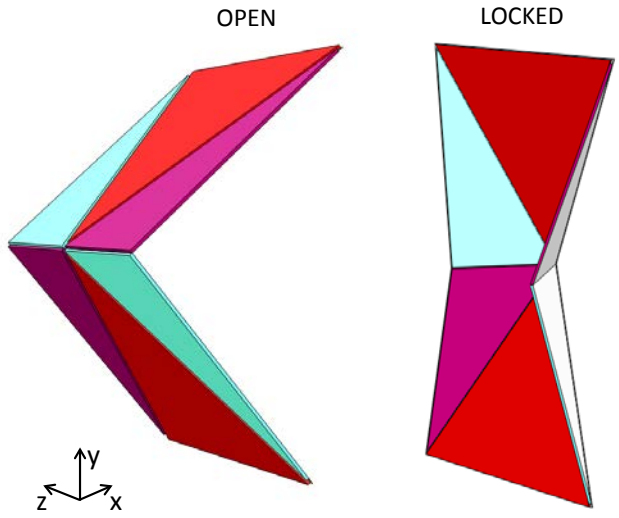

Figure 4. SINGLE SIDE DEPICTED IN OPEN AND LOCKED FORMS. NOTE THAT THE COLORING OF THE RIGID PANELS WILL REMAIN CONSISTENT THROUGHOUT THIS WORK FOR CLARITY

open state, the two horizontal mountain creases impede the motion of the diagonal valley creases on the pattern, and each side behaves as two flat plates connected by a simple middle hinge. However, once the angle between the upper and lower portion of the side exceeds 180°, the two center creases fold in as the side makes a "bowtie" shape, referred to herein as the *locked state*. If each side is in its locked state, the center vertices of all the sides converge in the middle of the structure and the two horizontal folds on each side converge in the center of each side, making the structure statically stable and capable of supporting vertical loads (this can be seen in Figure 1b-c).

3.1 State Analysis of Lateral Side

A detailed analysis of the structure requires first that the motion of a single side must be understood, in both open and locked states.

Assuming every fold is ideal (i.e. allows only for rotation along its axis and does not change from valley to mountain or vice versa), the motion of an open side is roughly equivalent to two rigid plates with a hinge in between them.

When a side is in its locked state, its motion is more complex, but can be understood through simplification of the center vertex of the side as a spherical mechanism, due to it being a series of panels connected by hinges intersecting at a common point. The spherical mechanism assumption is useful for analyzing the motion of origami mechanisms [13], particularly with waterbomb base-related origami [14], as it allows for an analytical understanding of the constraints and movement of every fold.

A unit sphere is first defined around the center vertex of the side, and the angles that determine the two panel shapes that constitute a side are defined as *q* and *s* (Figure 5). Assuming the side remains symmetric about a vertical axis, a relation can be derived between the input angle Φ of each panel *q*'s displacement and the output angles *A*, *B*, and *C* between the rigid panels. To do so, a spherical triangle is drawn between the two *s* panels (Figure 5). Since the side is symmetric, the lower two vertices *b* and *c* of the triangle will always fall along the same circle, whose radius can be defined by the chord, or straight line segment between two points on a circle, between the two vertices when the side is fully flat. Using the chord function, a function which outputs a chord distance between two points on a circle given the angle between those two points, the radius of the circle *b* and *c* lie on is then defined as

$$r = \sin(s) \tag{1}$$

The radius can then be used to find the chord between points *b* and *c* for any angular displacement Φ by applying the chord function again. This results in

$$a_{chord} = 2r\sin\left(\frac{180° - 2\Phi}{2}\right) = 2\sin(s)\sin(90° - \Phi) \tag{2}$$

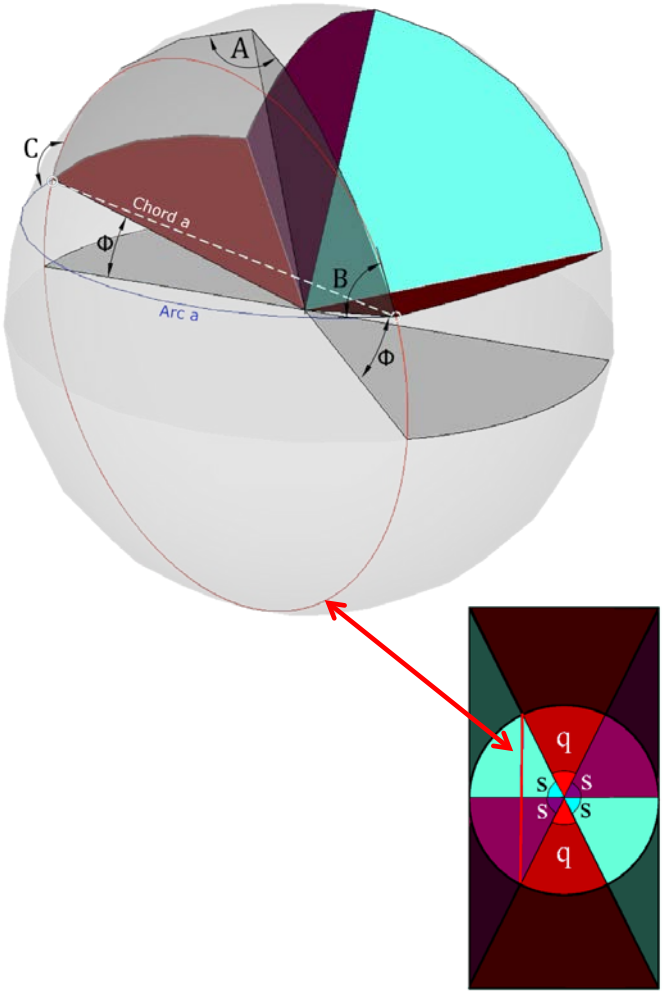

Figure 5. SPHERICAL REPRESENTATION OF CENTER VERTEX, WITH FLAT-FOLDED VERSION LAID OVER A SINGLE SIDE FOR REFERENCE

From equation (2), applying the inverse chord function yields an expression for the angular arc between the two points on the unit sphere

$$a_{Arc} = 2sin^{-1}[\sin(s)\sin(90° - \Phi)] \tag{3}$$

To fully define the state of the locked side, the angles *A* and *B* between the rigid panels must be known in relation to the input angle Φ. Once the a_{Arc} is known, angles *A*, *B*, and *C* can be defined using the cosine and sine rules of spherical trigonometry [15]

$$A = cos^{-1}\left[\frac{\cos(a_{Arc}) - cos^2(s)}{sin^2(s)}\right] \tag{4}$$

$$B = sin^{-1}\left[\frac{\mathrm{s} * \sin(\mathrm{A})}{a_{Arc}}\right] \tag{5}$$

Due to the symmetric assumption, angle C must equal angle B, thus the state of the side is known.

For the structure to support a static load with all sides in the locked state, the *s*-*s* folds (folds are designated by the panels bordering them, so *s*-*s* folds are the horizontal mountain folds) must meet at the same time the center vertices of all the

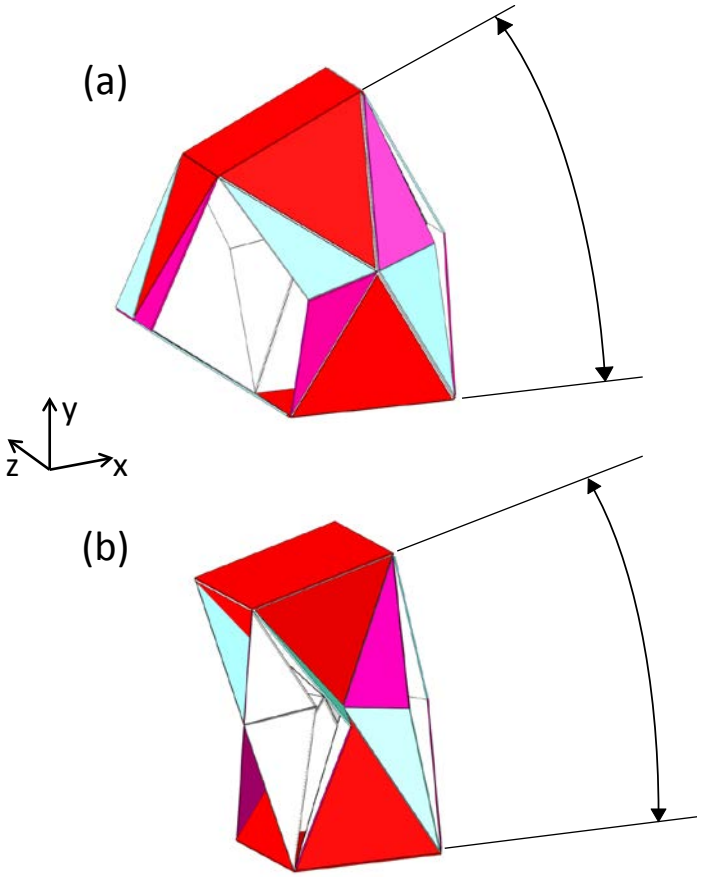

Figure 6. LIFTING STRUCTURE WITH NON-IDEAL FOLDS AT LARGE ANGLES OF Z ROTATION IN (a) FULLY OPEN AND (b) FULLY LOCKED STATES

sides meet in the center of the structure (see Figure 1c for clarity).This means the ratio of height *h* to width *w*, or aspect ratio (AR) is of great importance; too low of a height, and the vertices and *s*-*s* folds will not meet, rendering the structure unable to support load. For a square base, the locked state is most stable when both *s*-*s* folds of each side make contact along their entire length; this occurs when

$$h = 2w \tag{6}$$

Although this criterion is not necessary for the structure to operate, the locked form is most stable and can support the most weight when equation (6) is true, so an AR of 2:1 is recommended.

3.2 State Analysis of Complete Structure

Once the range of motion of a single side is quantified, the overall range of motion of the entire four-sided structure can be observed in greater detail. Knowledge of how the structure can move and its limitations is important for later actuation and control, so a brief overview of the structure's characteristics in the two states used for lifting a load is presented.

When all sides on the lifting structure are open, assuming folds are ideal the structure is functionally identical to a Sarrus linkage, having a single translational degree of freedom along the Y axis. However, with non-ideal folds, the *s*-*q* folds can transition to mountain folds and allow limited extra motion, providing five degrees of freedom; slight *X* and *Z* translation can occur, with coupled *Z* and *X* axis rotation, respectively. Figure 6a demonstrates this, depicting a fully open structure with a large degree of *Z* rotation on the upper base. In practical settings, this can permit lifting motion that is not perfectly level, and as such precise control of the system in a fully open state requires feedback of the angle between base panels.

When all sides are in a fully locked state, the structure possesses four degrees of freedom, as the upper base panel can translate in the *Y* direction as well as rotate along the *X*, *Y*, and *Z* axes. This range of motion stems from the ability of locked sides to compress or expand along the *Y* axis; one side can compress while the others expand to slightly change the angle of the upper base. This is illustrated in Figure 6b, which depicts a structure with all four sides locked rotating its upper base about the *Z* axis.

The extra motion that results from folds in the structure not behaving ideal in both states, it must be noted, is minimal compared to the greater magnitude motions that the ideal assumption predicts. In general, both fully open and fully locked states constrain the lifter to allow mainly only *Y* translation, the desired motion of actuation.

3.3 "Biasing" of Lateral Sides and Effects on Open-to-Locked Transition

Paper folded with a lateral side's crease pattern will naturally transition between the open and locked states with relative repeatability and ease; however, this design is intended to work with any well-selected combination of rigid panels and flexible substrate, and we discovered that in many cases, another stable but undesired state can occur instead of the locked configuration. To alleviate this, the rigid *s* panels were "biased" by extending their length a minute amount (referred to as *u*) over the *s*-*s* fold line (Figure 7). This section details the effect this has on the transition between open and locked states, from the angle at which it occurs to the energy required to initiate it.

In some cases during the transition between open and locked states, one of the *s* panels will continue to remain parallel with the adjacent *q* panel and buckle, rather than fold inwards towards the center of the side as in the normal locked

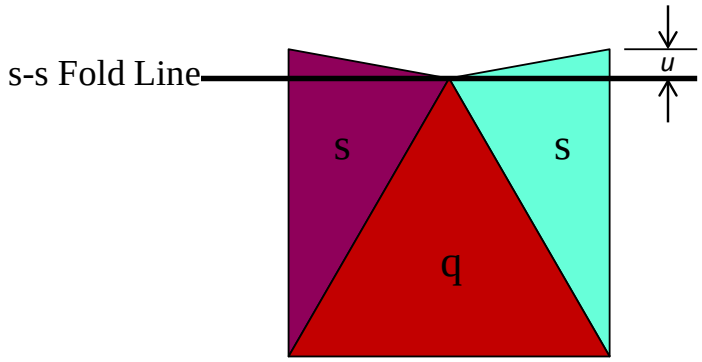

Figure 7. EXAGGERATED DEMONSTRATION OF RIGID PANEL BIAS ON LOWER HALF OF A LATERAL SIDE

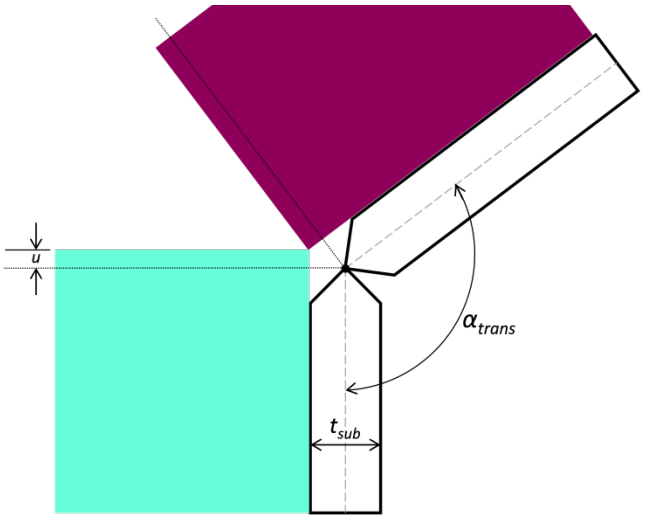

Figure 8. RELATION BETWEEN RIGID PANEL OFFFSET AND TRANSITION ANGLE

state. When this occurs angle *A* (see Figure 5) between the upper and lower *s* panels becomes greater than 180°. The intention of biasing the *s*-s folds is to constrain the lateral side in such a way that the undesired state cannot occur; by adding an extra length of rigid panel, angle *A* can be constrained to nearly reach, but not exceed, 180°, due to the rigid panels converging and blocking further motion. This constrains the angle *A* and prevents the undesired state.

There is a direct relationship between the extra length of rigid panel, which we will refer to as *u*, and the angle *A* at which the rigid panels converge and prevent further motion before transition between states (which we will refer to as the *transition angle*, or α_{trans}). To ease the derivation of this relationship, the flexible substrate is simplified to a small length flexural pivot [16], where, due to the length of the elastically deflecting substrate being significantly smaller than the rigid panel length, the substrate at the fold is assumed to behave as a pin joint located in the center of the fold (Figure 8). Through use of simple geometry, then, the relation between *u* and α_{trans} is found to be

$$\alpha_{trans} = 2tan^{-1}(t_{sub}/2u) \quad (7)$$

where t_{sub} is the thickness of the flexible substrate.

Biasing the fold with a rigid panel offset was found to increase the energy gap between stable open and locked states, which in turn increased the force required to transition between the two states. To understand why, a qualitative understanding can be found in an analysis of the potential strain energy stored in each fold of the side.

This energy can be determined by a method used previously for waterbomb-base origami [14, 17], where, as before, the flexible substrate is treated as a small length flexural pivot. Assuming no external work, the internal potential strain energy stored across a range of deflection is defined by

$$V = \frac{1}{2}k\theta^2 \quad (8)$$

where k is the stiffness of the bending portion of the substrate and θ is the angle of rotational deflection of the substrate. In the open state only the two *s*-*s* folds are deflecting, and as such the potential energy is expressed as

$$V = kA^2 \quad (9)$$

and, as before, *A* is the angle between the upper and lower *s* panels. For a locked side, all the folds are deflecting, and as such the potential energy can be written

$$V = kA^2 + 2k(180° - B - 2\Phi) \quad (10)$$

The term *(180°-B- 2Φ)* denotes the angle between *s* and *q* panels, expressed using terms that can be found with equations (1-5).

By non-dimensionalizing equations (9) and (10) by dividing all terms by *k*, any material-specific properties are removed and the plot in Figure 8 could be made to clarify the effect rigid panel bias has on the transition between open and locked states. The plot depicts *V/k* of a side in open and locked states across the range of angle *A*.

Ordinarily, with no rigid panel bias, the transition between open and locked states occurs at *A=180°*, where, as Figure 9 shows, there is a small energy gap between the two states that must be passed. When the rigid panel bias lowers the transition angle, it increases this gap. Figure 9 marks an example transition angle, where the gap between the two states is notably higher than it would be if the transition angle was 180°. This modifying of the energy difference between stable states is the main effect the rigid panel biasing can have on the structure, and understanding its effect is important in application of this design. If the rigid panel bias is made too large, then the transition between states becomes needlessly difficult. Too small, and the transition between open and locked states will not always occur.

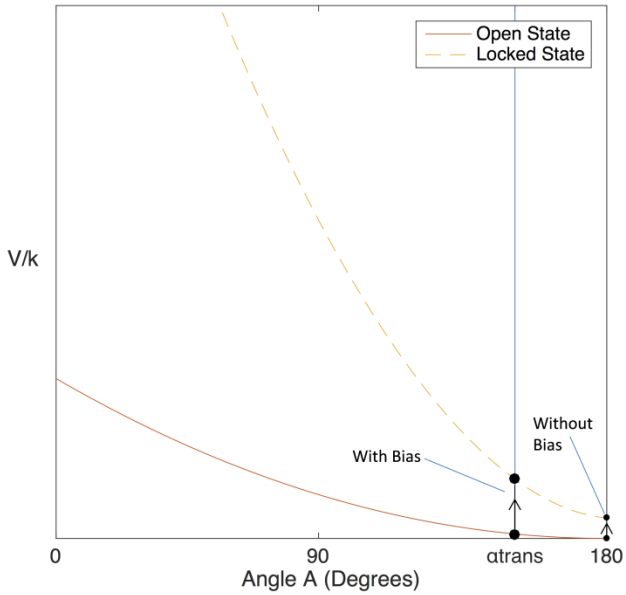

Figure 9. PLOT OF V/k VERSUS ANGLE A IN THE OPEN AND LOCKED STATES, WITH AN EXAMPLE TRANSITION ANGLE MARKED

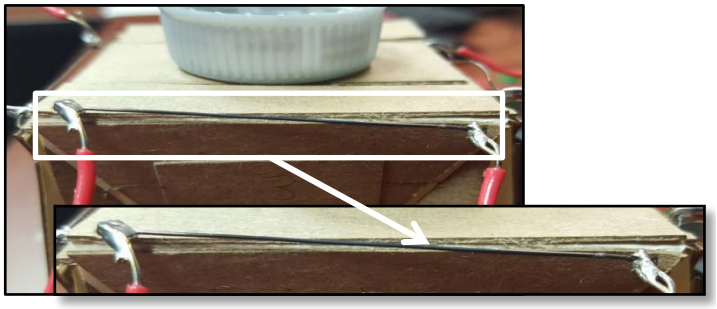

Figure 10. TORSIONAL SMA ELEMENT AFTER PLACEMENT IN PROTOTYPE STRUCTURE

4 ACTUATION

The structure is actuated using eight shape memory alloy (SMA) wires in torsion (shown in Figure 10), using a design similar to the one outlined by Koh, Kim, and Cho [18]. These wires are pre-strained by twisting them in the direction opposite of that desired during actuation and placed along the base folds connecting the lateral sides to the square bases of the structure, as in Figure 11. SMA wire is commercially available and simple to operate in torsion, and it integrates well into origami folds as a means to produce torque along folds while allowing the planar form factor of origami to be retained. It is important to note that wires pre-strained in the lifting direction are not strictly necessary; later designs could incorporate wires pre-strained to provide torque opposite the lifting direction for reversible actuation.

Although the SMA wire could be embedded along any of the folds in the structure, for the structure to be fully controllable the angle of the actuated folds must affect the state of the structure in both the open and locked forms; this criteria precludes the actuation of the *s-q* folds, as their angle is constant in the open form. Of the remaining two options, the *s-s* folds and base folds, the base folds are far more preferable for SMA actuation for a number of reasons, chief of which being that the base fold angle for a given state of the structure is unique; there are no base fold angles which occur in both the open and locked states. This is opposed to the *s-s* folds, where the fold angle given by equation (4) has a range of values found in both the open and locked states. By placing the SMA wire along the base folds, then, a torque applied by the wire directly correlates to a change in fold angle and therefore change in state of the entire structure.

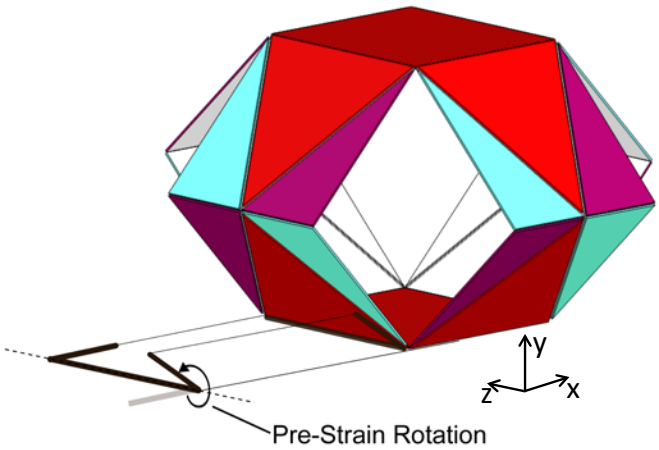

Figure 11. PRE-STRAIN ROTATION ABOUT Z AXIS AND PLACEMENT OF SMA WIRE. THE GHOST IMAGE OF THE WIRE REPRESENTS ITS UNSTRAINED SHAPE

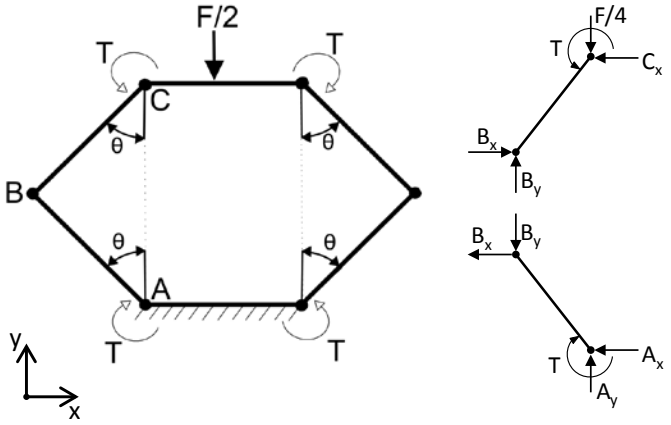

Figure 12. TWO DIMENSIONAL STATIC ANALYSIS OF STRUCTURE.

A useful actuator must be able to hold a load static at a given height. Understanding the torque required from each SMA wire to do so is key to creating a better control system for this design. To create a general approximation of the relationship between the torque produced by the SMA wires and the load they are capable of lifting, an analysis of the statics of the structure must be performed. It must be noted that the following model is a basic simplification of the structure, and does not account for self-weight, nor does it consider structural dynamics; it is intended to aid in the selection of SMA wire and to gain valuable understanding of the structure in different states of static equilibrium.

Applying the earlier assumptions that folds are ideal (i.e. allowing only rotation about fold lines and no changing from valley to mountain folds or vice versa), a free body diagram can be drawn to represent two sides in the open state connected to both bases of the structure, as in Figure 12. Although the *Z* direction of the structure is not represented, the ideal fold assumption implies that the angles θ are equal and both bases parallel. This makes the structure symmetric; all sides will experience the same forces and the relationship between actuator torque and load on the whole structure can be understood from analysis of a single side. This symmetry is also why *F*, the load force on the structure, is halved in the free body diagram; only two sides are being analyzed.

Isolating a single open side, it can be separated into two links AB and BC connected by a pin joint as in Figure 12. Taking the summation of moments about points C and A in static equilibrium, the equations

$$\sum M_A = 0 = -T + B_x \frac{h}{2} cos\theta + B_y \frac{h}{2} sin\theta \qquad (11)$$

$$\sum M_C = 0 = T + B_x \frac{h}{2} cos\theta - B_y \frac{h}{2} sin\theta \qquad (12)$$

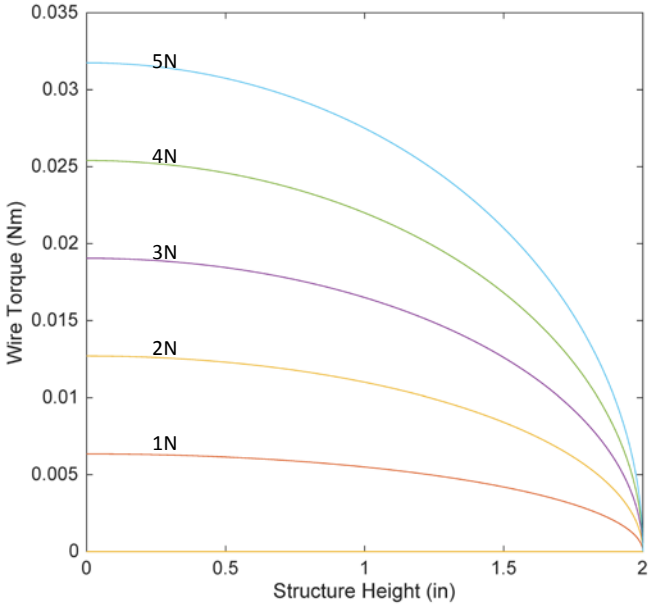

Figure 13. PLOT OF INDIVIDUAL WIRE TORQUE VS. STRUCTURE HEIGHT AT VARIOUS LOADS DESIGNATED ON GRAPH

are found, where T is the torque produced by a single SMA wire, B_x and B_y are the reaction forces at pin B, and moments are positive in the counter-clockwise direction. Isolating a single segment BC and summing the forces in the Y direction, one obtains

$$B_y = F/4 \tag{13}$$

where F is the total load on the structure. By setting equations (11) and (12) equal to each other and substituting equation (13) into both, the relation

$$T = \frac{Fh}{8} sin\theta \tag{14}$$

is determined.

Equation (14) shows that as θ decreases and the structure height increases, less torque is required from each SMA wire to hold a given load static. This is presented in Figure 13, which plots the torque required to hold a range of loads from 0N to 5N static at different heights, using equation (14). It can be seen that no torque is required to hold a load once the max height is reached; at that point, the structure transitions to the locked state, where no additional power input is required. It can also be seen that the structure requires the greatest amount of torque to lift when it is flattest. If the structure is to hold a load at a certain height, it would be preferable to design the structure so that height is close to its maximum height.

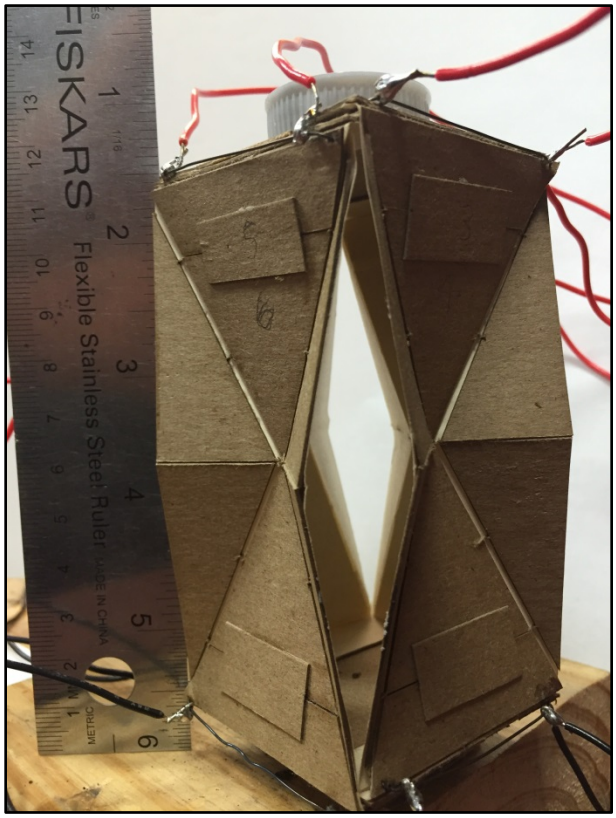

Figure 14. IMAGE OF PROOF-OF-CONCEPT PROTOTYPE

5 EXPERIMENTAL APPROACH

A physical prototype of the design with 2 x 1 inch (5.08 x 2.54 cm) sides, as shown in Figure 14, was fabricated to serve as a proof-of-concept and as a test bed for evaluating design performance. The structure was made using laser-cut cardstock panels adhered onto a paper substrate. Each side was produced separately then connected to the bases through hinges with the SMA wire preinstalled; this allowed the SMA elements to be embedded independently, without disturbing other parts of the structure.

The actuation of the structure is achieved by heating one SMA wire at a time, quickly cycling through the eight total wires to achieve actuation with less power required than heating all wires simultaneously in parallel. To do this, a bank of MOSFET transistors is wired in parallel to a power supply and controlled by a National Instruments myRIO processor sending digital control signals to the MOSFETs. Each MOSFET is tied to an individual SMA wire on the structure, so when a control signal is received by the MOSFET, current is provided to the corresponding SMA wire (Figure 15). A LabView program implements the block diagram of Figure 16 and directs the myRIO to send a digital Pulse Width Modulated (PWM) signal to a desired MOSFET. The 3.3V PWM control signal is higher than the MOSFET's gate threshold voltage of 1-2.5V and thus opens the MOSFET to supply power to the desired SMA wire. The PWM frequency utilized for our control system was 20 kHz, chosen primarily because higher frequency signals allow faster switching of the MOSFETs, which translates to smoother operation of the lifting structure overall.

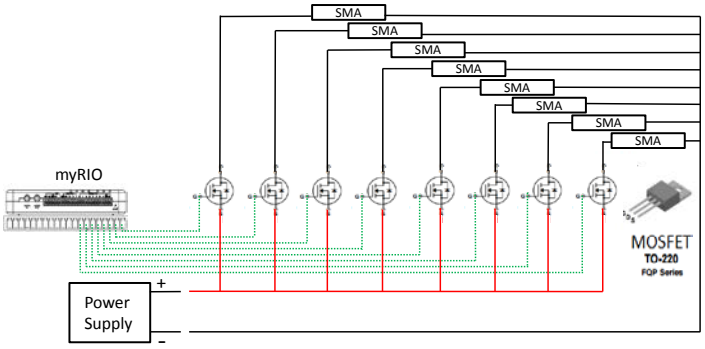

Figure 15. SCHEMATIC OF CONTROL SETUP

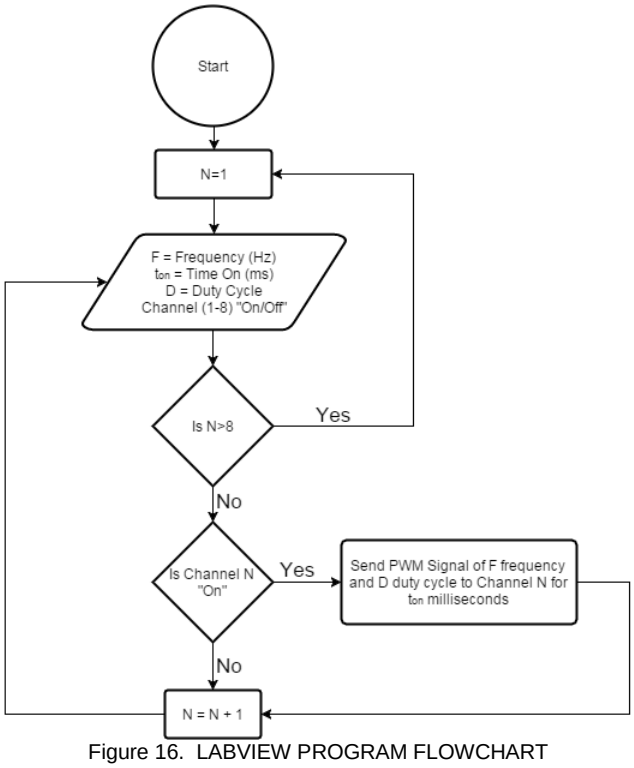

Figure 16. LABVIEW PROGRAM FLOWCHART

The myRIO board contains eight digital outputs, each tied to send a PWM signal to a particular MOSFET/SMA wire pair. As the control program cycles through the eight output channels, it supplies current (using the MOSFETs) through each individual SMA wire for a span of time t_{on} specified by the user. The value of t_{on} had a significant impact on the lifting characteristics of the structure, as it determined the length of time current was applied to each SMA wire as well as how long a wire would sit idle before current would be applied to it again (as current is applied to wires one at a time). This meant t_{on} determined the rate at which SMA wires gained temperature and actuated, making it the main parameter changed when fine-tuning the control of the structure.

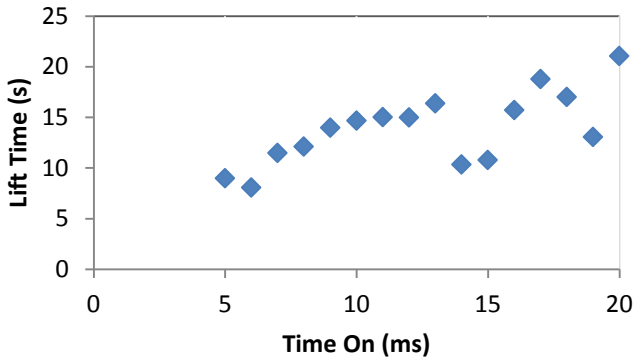

Figure 17. PLOT OF LIFT TIME VS. TIME ON (t_{on}) VALUES

6 RESULTS

Once fully built, the test structure (not including the wires leading to the MOSFET board) weighed a total of 22g, yet was able to lift weights of up to 100g before failure. The failure mode was the inability of the upper platform of the structure to remain parallel with the lower platform, allowing test weights to slide or fall off the structure. Improved construction with less flexible and more constraining substrate materials could alleviate this problem by better constraining folds to allow only axial rotation.

The structure demonstrated the ability to statically support loads exceeding lifted load, and could freely support up to 200g without any input. Upon adding more load, its locked form would become rotationally unstable about the *X* and *Z* axes—a behavior that we believe could be corrected with better selection of materials and precision of construction. The structure demonstrated a fastest actuation time of 8 seconds to lift a 50g mass, occurring at t_{on} = 6ms, F = 20kHz, and a voltage input of 2.5V.

As discussed in Section 5, the control scheme used for this structure allowed the amount of time spent heating each wire during a cycle, t_{on}, to be initially set; this value has large effects on the behavior of the structure, as different time on values mean different heating and cooling rates for the SMA wire, and therefore different actuation times for the structure. Finding an ideal time on value for the structure was important for obtaining the best possible performance, so the time required for the structure to go from fully flat to fully locked was recorded for t_{on} values ranging from 5 to 20ms. The results of this test make up the plot shown in Figure 17. Values below 5ms were not recorded as they could not consistently lift a 50g mass in a useful amount of time (under 1 minute).

Figure 17 allowed an ideal t_{on} value to be located at 6ms. Most of the data followed a consistent trend of higher t_{on} corresponding to higher lift time. We suspect this was due to the higher t_{on} values being poorer suited for the heating/cooling cycle on each individual wire; although a higher t_{on} provides a longer heating time, it also causes a greater amount of idle unheated time between cycles, resulting in less overall

temperature gain in the wire per cycle than shorter t_{on} values provide. This slowed down the actuation process for many of the higher t_{on} values, resulting in the upward trend. When t_{on} was in the 14-15ms and 18-19ms ranges, however, there was an improved performance relative to nearby values. The amount of heat dissipation and heat generation during a cycle for these outlier ranges is not significantly different from nearby t_{on} values with longer actuation times. We have reason to suspect the response of the SMA actuators is merely inconsistent, as the SMA wires used were not trained to stabilize their response. Further investigation would require careful measurement of wire temperature and phase transition, outside of the scope of this paper.

7 CONCLUSIONS AND FUTURE WORK

To fulfill a noted gap in origami engineering, and to help demonstrate the capability of performing "useful" work, we presented the basic concept and design for an origami-inspired mechanism capable of lifting and supporting a load. The basic geometry and design requirements were set forth, as was the preferred actuation method and proof-of-concept construction, and these were analyzed to provide further insight for improving this design and adapting it for later uses.

Analysis of the structure and geometry of the design in Section 3 showed that rigid panel biasing of the lateral sides, although necessary to prevent undesired states, can increase the amount of force required to transition between open and locked states. Any application of this design will have to properly balance the rigid panel offset to the needs of the application, constraining sides into only the open and locked states while not increasing the force required to transition significantly.

Construction and testing of a prototype design demonstrated the feasibility and potential of the design. The prototype showed it was capable of all the abilities initially desired; using an origami design to lift a mass and then supporting the same mass with no power input, all within reasonably quick actuation times of less than 20 seconds. The open-loop control method proved to work as a preliminary system, and was shown to operate best at lower values of t_{on}. We conclude, then, from the proof of concept structure that there is useful merit to this design as an actuator.

Although the proof of concept of this design performed well, future work has room for improvement in actuation, structural strength, and control. Using the tools and models shown in this paper, the design can be improved and abilities like reversible actuation and precise height control are achievable. As a result, future work on this design will center on improving control and construction of the design, as well as further investigating the stability and strength trade-offs of different base configurations and forms. There is also no limitation to the number of sides used for this design; the use of four sides in this paper is an arbitrary choice. Structures with different configurations of sides have different behaviors, strengths, and weaknesses, and provide an avenue for further work and exploration.

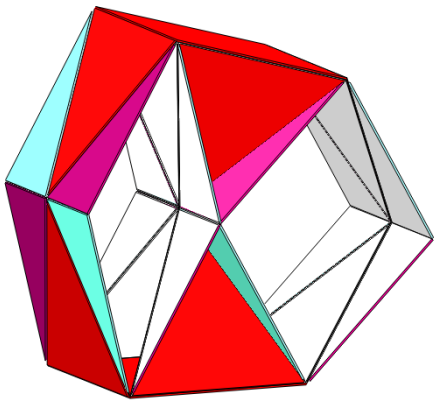

Figure 18. HIP JOINT CONFIGURATION OF STRUCTURE

Additionally, this work only observed two states of the origami structure; all sides open, and all sides locked. There is a variety of combinations of open and locked sides that are available, and each combination has its own applications and design uses. An example configuration is shown in Figure 18, where opposite pairs of locked and open sides can form a hip joint.

We believe the potential uses of this design are varied, as a lightweight, flat-folding actuator could provide a useful alternative for engineers in a variety of applications, particularly in aerospace, where low footprint and weight are paramount. Our hope is by improving this concept, and providing the necessary information to optimize it for different situations and uses, it can become a useful option for engineers around the world.

ACKNOWLEDGMENTS

Many thanks go to Rodney Inmon and John Rohmer for their help in building the proof-of-concept, as well as the help from Edwin Peraza Hernandez.

This material is based upon work supported by the National Science Foundation under the "Origami Design for Integration of Self-Assembling Systems for Engineering Innovation" (ODISSEI) program, grant EFRI-1240483. Opinions expressed in this paper are of the authors and do not necessarily reflect the views of the National Science Foundation.

REFERENCES

[1] Tang, R., Huang, H., Tu, H., Liang, H., Liang, M., Song, Z., Xu, Y., Jiang, H., and Yu, H., 2014, "Origami-Enabled Deformable Silicon Solar Cells," Applied Physics Letters, 104(8), pp. 083501.

[2] Cromvik, C., and Eriksson, K., 2006, "Airbag Folding Based on Origami Mathematics," Proc. Origami4: Fourth International Meeting of Origami Science, Mathematics, and Education, pp. 129-139.

[3] Filipov, E. T., Tachi, T., and Paulino, G. H., 2015, "Origami Tubes Assembled into Stiff, yet Reconfigurable Structures and Metamaterials," Proceedings of the National Academy of Sciences, 112(40), pp. 12321-12326.

[4] Lee, D.-Y., Kim, J.-S., Kim, S.-R., Koh, J.-S., and Cho, K.-J., 2013, "The Deformable Wheel Robot Using Magic-Ball Origami Structure," ASME Paper No. DETC2013–13016.
[5] Zhakypov, Z., Falahi, M., Shah, M., and Paik, J., 2015, "The Design and Control of the Multi-Modal Locomotion Origami Robot, Tribot," Proc. Intelligent Robots and Systems (IROS), 2015 IEEE/RSJ International Conference on, pp. 4349-4355.
[6] Hawkes, E., An, B., Benbernou, N., Tanaka, H., Kim, S., Demaine, E., Rus, D., and Wood, R., 2010, "Programmable Matter by Folding," Proceedings of the National Academy of Sciences, 107(28), pp. 12441-12445.
[7] Peraza-Hernandez, E. A., Hartl, D. J., Malak Jr, R. J., and Lagoudas, D. C., 2014, "Origami-Inspired Active Structures: A Synthesis and Review," Smart Materials and Structures, 23(9), pp. 094001.
[8] Martinez, R. V., Fish, C. R., Chen, X., and Whitesides, G. M., 2012, "Elastomeric Origami: Programmable Paper-Elastomer Composites as Pneumatic Actuators," Advanced Functional Materials, 22(7), pp. 1376-1384.
[9] Escrig, F., and Brebbia, C. A., 1996, Mobile and Rapidly Assembled Structures Ii: Second International Conference on Mobile and Rapidly Assembled Structures, Maras 96, Computational Mechanics.
[10] Kim, J., Lee, D.-Y., Kim, S.-R., and Cho, K.-J., 2015, "A Self-Deployable Origami Structure with Locking Mechanism Induced by Buckling Effect," Proc. Robotics and Automation (ICRA), 2015 IEEE International Conference on, pp. 3166-3171.
[11] Onal, C. D., Wood, R. J., and Rus, D., 2013, "An Origami-Inspired Approach to Worm Robots," Mechatronics, IEEE/ASME Transactions on, 18(2), pp. 430-438.
[12] Salerno, M., Zhang, K., Menciassi, A., and Dai, J. S., 2014, "A Novel 4-Dofs Origami Enabled, Sma Actuated, Robotic End-Effector for Minimally Invasive Surgery," Proc. Robotics and Automation (ICRA), 2014 IEEE International Conference on, pp. 2844-2849.
[13] Bowen, L. A., Grames, C. L., Magleby, S. P., Howell, L. L., and Lang, R. J., 2013, "A Classification of Action Origami as Systems of Spherical Mechanisms," Journal of Mechanical Design, 135(11), pp. 111008.
[14] Hanna, B. H., Lund, J. M., Lang, R. J., Magleby, S. P., and Howell, L. L., 2014, "Waterbomb Base: A Symmetric Single-Vertex Bistable Origami Mechanism," Smart Materials and Structures, 23(9), pp. 094009.
[15] Chiang, C.-H., 1988, Kinematics of Spherical Mechanisms, Cambridge University Press Cambridge.
[16] Howell, L. L., 2001, Compliant Mechanisms, John Wiley & Sons.
[17] Bowen, L., Springsteen, K., Feldstein, H., Frecker, M., Simpson, T. W., and Von Lockette, P., 2015, "Development and Validation of a Dynamic Model of Magneto-Active Elastomer Actuation of the Origami Waterbomb Base," Journal of Mechanisms and Robotics, 7(1), pp. 011010.
[18] Koh, J.-S., Kim, S.-R., and Cho, K.-J., 2014, "Self-Folding Origami Using Torsion Shape Memory Alloy Wire Actuators," Proc. ASME 2014 International Design Engineering Technical Conferences and Computers and Information in Engineering Conference, pp. V05BT08A043-V05BT08A043.